Effects of Polyester-Poor Phase Microstructures on Viscosity Development of Polymer Blends

Young Gyu Jeong, Natalia V. Pagodina, Cuihong Jiang, and Shaw Ling Hsu*

Polymer Science and Engineering Department and Materials Research Science and Engineering Center, University of Massachusetts, Amherst, Massachusetts 01003

Charles W. Paul

National Starch & Chemical, Bridgewater, New Jersey 08807

Received March 24, 2006; Revised Manuscript Received May 11, 2006

ABSTRACT: The viscosity development associated with the microstructure of various crystallizable polymer blends has been investigated. All binary blends, consisting of crystallizable polyester and noncrystallizable polyether, exhibit liquid/liquid phase-separated structures with polyester-rich and polyester-poor phases. The dispersed domains−continuous matrix morphology was observed in blends with 10−40 wt% polyester, while the 50 wt% polyester blend exhibits bicontinuous morphology. Differential scanning calorimetry and optical microscopy were employed to characterize crystallization features of each phase. "Curve-leaf"-shaped crystallites were formed in the polyester-poor phase in all blends studied. The viscoelastic physical gelation of the phase-separated blends with low polyester content of 10−40 wt% was found to be dominated by crystallization in the polyester-poor phase. The unusually high viscosity of the polyester-poor phase is due to the percolated morphology of "curved leaf"-shaped crystallites.

Introduction

Polymer blends have been studied extensively from both fundamental and practical perspectives. Each polymer component has unique characteristics which, when blended, lead to improved physical properties, ease in processing, and perhaps lower cost.[1−3] Our research focused specifically on crystallizable blends which may be used in a number of coating or adhesive applications.[4] The aliphatic polyesters are employed to control viscosity and mechanical property through crystallization; the polyethers provide elasticity and impact strength. In our case, the third component of acrylic copolymers with high glass transition temperature is included to improve melt strength at elevated temperature.[5,6] Our initial studies focused on phase behavior of various blends. Even small changes in chemical structure were found to lead to tremendous differences in phase behavior.[6,7] The increased understanding of phase behavior subsequently led to a comprehensive analysis of crystallization kinetics in various regions of phase-separated structures. As expected, crystallization in the polyester-rich regions and especially at interfaces starts quickly. The crystallization kinetics and achieved degree of crystallinity depend on the overall sample composition and localized chain dynamics.

As mentioned above, these ternary blends are used extensively in coating and adhesive applications. Processing parameters such as viscosity control as a function of time for blends of varying composition and at different temperatures are important considerations. Polyester crystallinity was found to have a profound influence in the multistep solidification process.[8] Information on evolving microstructural features (liquid/liquid phase-separated structure, crystallinity, crystalline morphology, etc.) is extremely important and necessary. Although the overall crystallization kinetics of ternary blends has been analyzed, the crystallization process in rich and poor compositions has yet to be individually characterized. Ternary blends can be extremely complex in some cases. There is no question that the acrylates used are important as they control overall segmental mobility. Their effects can be seen in both phase separation behavior and localized crystallization kinetics. Because of different functional groups used in forming acrylate copolymers, the specific interaction of the three components can also change the overall miscibility phase diagram.[6] To reduce the complexity of the system to be studied, we focused on binary blends of polyester with polyether.

Polymer blends in general are thermodynamically immiscible. Therefore, the domain structure and interfacial properties in the phase-separated blends are important factors to viscoelastic properties. Also, when cooled below the thermodynamic melting temperature, the crystallizable polymer blends undergo crystallization. There, the microstructural evolution and features in the crystallizable binary or ternary blends is complex since liquid/liquid phase separation and crystallization may undergo concurrently. Depending on the components in miscible or immiscible crystallizable/noncrystallizable blends, the miscibility and associated phase diagrams were found to be totally different.[6,7,9] The microstructural evolution and features of those blends were also characterized.[10] Depending on the local composition of crystallizable polymer in those binary blends, the crystallization kinetics and degree of crystallinity differed dramatically,[10] which eventually influences curing kinetics and viscoelastic mechanical properties.[5,11]

For various homopolymers[12−14] and copolymers,[15−17] the crystallization process represents a physical gelation from the melt to solid state. This is characterized by a gradual change in the material viscoelastic response. A definitive relationship correlating the evolving morphological features and the viscoelastic response remains missing, however, especially for immiscible and crystallizable polymer blends. A single microstructural model of the immiscible and crystallizable polymer blends cannot account for the evolution of the viscoelastic

* To whom correspondence should be addressed: Tel 413-577-1125; Fax 413-545-0082; e-mail slhsu@polysci.umass.edu.

10.1021/ma060666z CCC: $33.50
Published on Web 06/14/2006

properties over the entire process. Morphological factors which influence the viscoelastic mechanical response of immiscible and crystallizable blends include (1) size, distribution, and shape of the dispersed phase in the liquid/liquid phase-separated structure,[18−21] (2) viscosity ratio and interfacial characteristics between two phases,[18,19,22−24] and (3) crystalline microstructural features (crystallinity and crystalline shape) developed by crystallization.[13,21]

In the current study, we investigated the effects of microstructural evolution and features (liquid/liquid phase-separated structure, interaction between two phases, degree of crystallinity, and crystallite shape) on the viscoelastic gelation behavior in immiscible and crystallizable binary blends. Poly(hexamethylene adipate) (PHMA) was employed as a crystallizable aliphatic polyester and poly(propylene glycol) (PPG) as a noncrystallizable polyether for the model binary blend exhibiting both liquid/liquid phase separation and crystallization. The local composition was characterized using ^{1}H NMR spectroscopy. Viscosity development of the binary blends with a variety of compositions was characterized using rheometry. The abrupt changes in sample viscosity have been directly correlated to the crystallization behavior of the polyester poor phase. Our results are reported here.

Experimental Section

Materials and Blends. Crystallizable poly(hexamethylene adipate) [PHMA, number-average molecular weight (M_n) = 1575 g/mol, polydispersity index (PDI) = 1.59, melting temperature (T_m) = 55 °C, glass transition temperature (T_g) = −61 °C] and noncrystallizable poly(propylene glycol) (PPG, M_n = 1887 g/mol, PDI = 1.01, T_g = −66 °C) were utilized for the immiscible and crystallizable binary blends. PHMA and PPG have primary and secondary hydroxyl groups at their chain ends, respectively.

PHMA/PPG binary blends with compositions of 10, 15, 20, 25, 30, 40, and 50 wt% PHMA were prepared in glass vials by melt-mixing at 120 °C. These blends were first dried under high vacuum and then placed in a temperature-controlled oven purged with nitrogen to minimize oxidative degradation. All blends at 120 °C were mixed periodically and quenched into liquid nitrogen. A typical optical morphology of PHMA/PPG blends is shown in Figure 1A, which exhibits phase-separated morphology with PHMA-rich phase and PHMA-poor phase. Another set of blends was allowed to phase-separate into two layers at 120 °C until the phase of the blends remained unchanged, as shown in Figure 1B. The top and bottom layers are PHMA-poor and PHMA-rich phases, respectively. The blends phase-separated in two layers were quenched to collect each phase. For all binary blends as well as PHMA-rich and PHMA-poor phase samples, the composition, morphological features, crystallization kinetics, and rheometric properties were characterized.

Optical Microscopy. Morphological features of blends such as phase-separated structure and crystallites were characterized using an Olympus Vanox optical microscope equipped with a hot stage and digital camera. Specimens were prepared by melting the blends between two glass slides on a hot stage at 120 °C for 2 min. Optical micrographs of the blends were recorded by lowering temperature from 120 to 35 °C. The appearance of crystals can be observed between two polarizers with an orthogonal polarization axis.

^{1}H NMR Spectroscopy. The local composition of each PHMA-rich and PHMA-poor phase in the phase-separated blends was analyzed using ^{1}H NMR spectroscopy. A Bruker DPX300 spectrometer was used to record spectra. Sample concentration was controlled to ∼20 mg/mL in $CDCl_3$.

Differential Scanning Calorimetry. Sample crystallization and melting behavior were studied using a differential scanning calorimeter (DSC Q100, TA Instruments, Inc.). Samples were heated to 120 °C, held for 2 min, and then rapidly cooled to predetermined crystallization temperatures (T_c) of 35−45 °C.

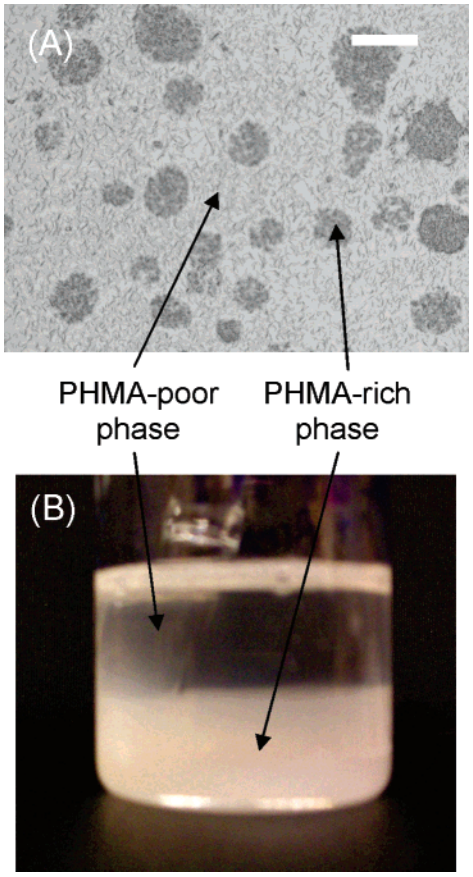

Figure 1. (A) A typical morphology of the PHMA/PPG blend after mechanical mixing for 5 min at 120 °C. The scale bar is 100 μm. (B) The PHMA/PPG blend with same composition as sample (A) after holding for 24 h at 120 °C.

Isothermal crystallization at each crystallization temperature was monitored by the heat flow of crystallization as a function of time. Following isothermal crystallization at a given crystallization temperature, the sample was heated to 120 °C at the heating rate of 10 °C/min. The degree of crystallinity of a sample at each crystallization temperature was calculated by comparing the measured melting enthalpy (ΔH_m) with the equilibrium melting enthalpy (ΔH_m° = 151 J/g) of PHMA.[25]

Rheometry. Temperature- and time-dependent viscosity development of samples due to quiescent crystallization was measured with by small-amplitude oscillatory shear by use of the cone and plate geometry of the Advanced Rheometric Expansion System (ARES, Rheometric Scientific Inc.). The instrument was operated using RSI Orchestrator version 6.3.0. To avoid strain-induced crystallization, frequency and applied strain were controlled at 1 rad/s and 1%. The samples were first melted at 120 °C for 2 min and then cooled to predetermined temperatures of 35−45 °C. The complex viscosity (η^*) was monitored as a function of time and temperature.

Results and Discussion

Morphology, Local Composition, and Blend Crystallization. PHMA/PPG binary blends are immiscible for all compositions prepared in this study. All samples exhibit phase-separated structures composed of PHMA-rich and PHMA-poor phases, as shown in Figure 2. Composition distribution in each phase was analyzed using micro-Raman techniques.[10] Chemical mapping of the relative polyester−polyether content in each phase can be established with high spatial resolution (∼1 μm). Blends with PHMA content from 10 to 40 wt% display a typical morphology of dispersed PHMA-rich phase domains and continuous PHMA-poor phase (Figure 2A−D). The domain size

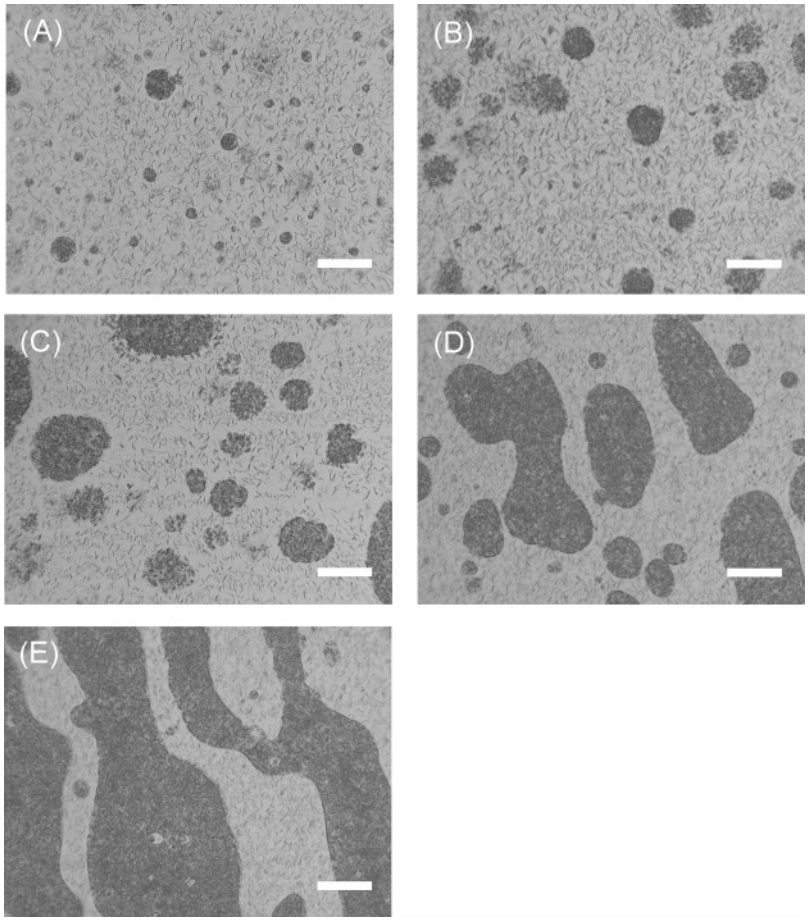

Figure 2. Optical micrographs of PHMA/PPG blends with various compositions at 25 °C: (A) 10 wt% PHMA, (B) 20 wt% PHMA, (C) 30 wt% PHMA, (D) 40 wt% PHMA, and (E) 50 wt% PHMA. The scale bar is 100 μm.

Table 1. Overall and Local Compositions of PHMA/PPG Blends

PHMA content in blends		PHMA content in PHMA-rich phase		PHMA content in PHMA-poor phase	
wt %	mol %	wt %	mol %	wt %	mol %
10	2.75	74.0	42.0	5.65	1.50
15	4.30	73.5	41.4	5.77	1.62
20	5.98	71.6	39.1	7.84	2.12
25	7.82	70.7	38.0	8.74	2.38
30	9.83	68.3	35.4	9.73	2.67
40	14.5	65.0	32.1	11.0	3.05
50	20.3	60.6	28.1	12.2	3.42

of the PHMA-rich phase increased with increasing PHMA. In contrast, the blend with PHMA content of 50 wt% shows bicontinuous morphology where each PHMA-rich and PHMA-poor phase is connected continuously, as seen in Figure 2E.

Since these samples readily separate, it is possible to collect the samples on the two ends of the miscibility curve, the rich and poor phases.[6] The proton NMR technique is an excellent method to determine the composition in each phase (Figure 3). The intensities of peaks assignable to PPG (f, g, and h) are compared to PHMA signals (a, d, b + e, and c). This analysis is carried out for PHMA/PPG blends with a variety of compositions from 10 to 50 wt% of PHMA, as summarized in Table 1. The amount of PHMA in the PHMA-rich phase decreased slightly with increasing the overall PHMA content in the various binary blends (Figure 3A). The amount of polyester increased in the PHMA-poor phase with the overall PHMA content (Figure 3B). In theory, the composition of the two regions should not change as a function of the overall composition. Our results suggest that the miscibility of PHMA/PPG binary blends improved with increasing PHMA content in blends, i.e., composition-dependent miscibility behavior. Although a clear explanation is unavailable, similar behavior has been reported in other studies where binary blend miscibility was found to be dependent not only on temperature but blend composition as well.[26−28]

For all PHMA/PPG blend samples as well as each PHMA-rich and PHMA-poor phase sample, DSC experiments were conducted to characterize crystallization and the degree of crystallinity at crystallization temperatures from 35 to 45 °C. Upon quenching the sample from 120 °C to the various crystallization temperatures, the heat flow of sample crystallization was monitored as a function of time, as shown in Figure 4A. Crystallization rates decreased dramatically with increasing crystallization temperature in the range from 35 to 45 °C. After crystallization was achieved at a specific crystallization temperature, each sample was then heated to 120 °C to measure melting enthalpy, as shown in Figure 4B. The resulting degree of crystallinity of all PHMA/PPG blends is plotted as a function of blend composition, as seen in Figure 5, which shows a linear increase with PHMA content in blends for all crystallization temperatures. For a given blend, the overall degree of crystallinity decreased with increasing crystallization temperature. In the same fashion, the degree of crystallinity of the PHMA-rich or PHMA-poor phase was also analyzed. The degree of crystallinity of the PHMA-rich phase was found to decrease with increasing PHMA content in the blends, while that of the PHMA-poor phase increased, as seen in Figure 6. This result is expected, considering the PHMA content decreases in the PHMA-rich phase while increasing in the PHMA-poor phase with increasing overall PHMA blend content (Table 1).

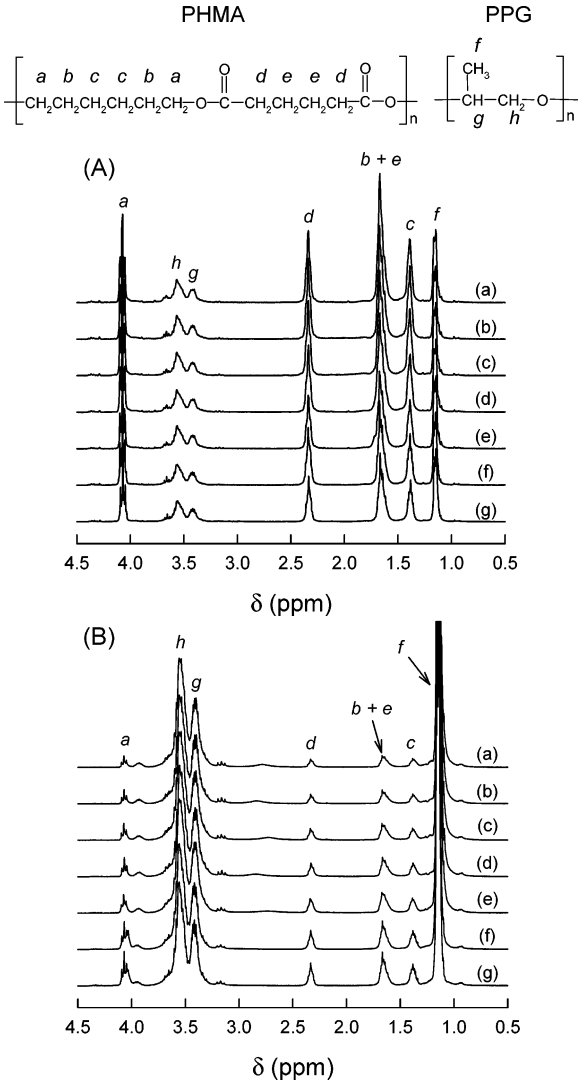

Figure 3. ^{1}H NMR spectra of (A) PHMA-rich phase and (B) PHMA-poor phase in PHMA/PPG blends with various compositions: (a) 10 wt% PHMA, (b) 15 wt% PHMA, (c) 20 wt% PHMA, (d) 25 wt% PHMA, (e) 30 wt% PHMA, (f) 40 wt% PHMA, and (g) 50 wt% PHMA.

Viscoelastic Gelation Behavior Associated with Microstructural Evolution. The viscosity change upon sample cooling from 120 °C to various temperatures of 35−45 °C has also been characterized for all PHMA/PPG blends (10−50 wt% PHMA) listed above. The representative time−temperature viscosity changes are shown in Figure 7. For blends with 10−40 wt% PHMA, the viscosity development is slower with increasing the temperature in the range from 35 to 45 °C (Figure 7A−C). The ultimate measured viscosity is lowered with increasing temperature (Figure 8). At a specific crystallization temperature, viscosity development is faster with increasing PHMA content in the blends (Figure 7A−C), and the ultimate achieved viscosity is higher (Figure 8).

As we demonstrated previously, this rise in blend viscosity in the cooling process from 120 °C to various crystallization temperatures can be directly correlated to PHMA crystallites formation. It can therefore be concluded that the time-dependent viscosity development is consistent with the crystallization behavior of the blends. It should be noted that the blend with 50 wt% PHMA exhibits different viscosity development from other samples. The viscosity value of the blend with 50 wt% PHMA is saturated at all crystallization temperatures of 35−45 °C (Figure 7D), indicating that, unlike other blends containing

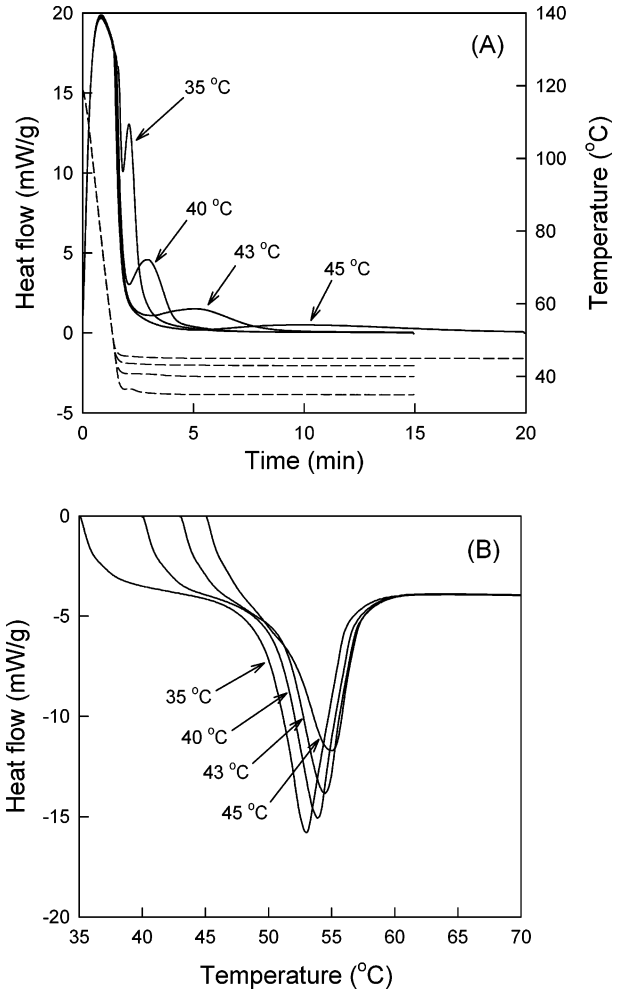

Figure 4. (A) Typical heat flow of crystallization as a function of time for PHMA/PPG blends crystallized isothermally at various temperatures of 35−45 °C. Dashed lines indicate temperature profiles from 120 °C to each crystallization temperature. (B) Typical heat flow of melting as a function of temperature for PHM/PPG blends crystallized isothermally at various temperatures of 35−45 °C.

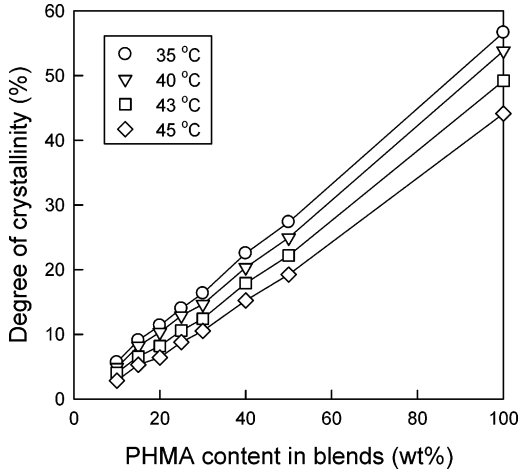

Figure 5. Degree of crystallinity of PHMA/PPG blends and PHMA homopolymer crystallized isothermally at various temperatures of 35−45 °C.

10−40 wt% PHMA, the sample is fully solidified. It is also interesting to note that, although the degree of crystallinity (19.2%) of the blend with 50 wt% PHMA crystallized at 45 °C is lower than that (22.5%) of the blend with 40 wt% PHMA at 35 °C, the ultimate viscosity of the former is higher. This

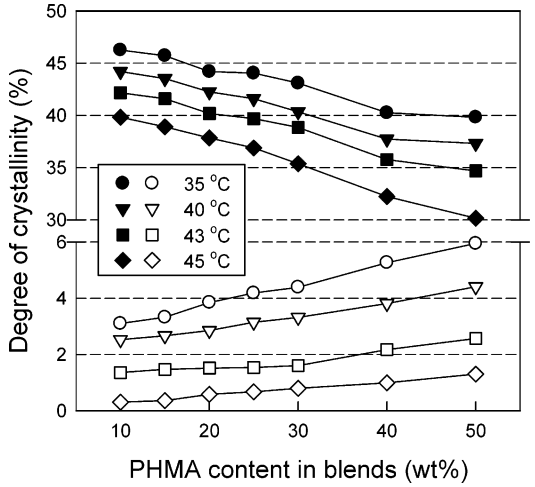

Figure 6. Degree of crystallinity of the PHMA-rich phase (filled symbols) and PHMA-poor phase (open symbols) for PHMA/PPG blends crystallized isothermally at various temperatures of 35−45 °C.

result is believed to stem from the bicontinuous morphology found for this sample (Figure 2E), which is quite different in comparison to the morphology of other blends (Figure 2A−D). This result is consistent with previous reports showing that bicontinuous and interpenetrating domain structures can indeed be associated with high viscosity in polymer blends.[29]

In phase-separated PHMA/PPG blends, the crystallization process occurs in both PHMA-rich and PHMA-poor phases at different rates and to different degrees (Table 1, Figure 6). One may question how the crystallization process in each phase contributes to the viscosity development of the phase-separated blends. To investigate the relative contribution of the two types of semicrystalline regions, PHMA domains and PHMA-poor matrix, to viscoelastic development of the overall sample, the two types of samples were investigated separately. The time-dependent viscosity development of the PHMA-rich and PHMA-poor phases, obtained for the blend with 10 wt% PHMA, is shown in Figure 9. For the PHMA-rich phase in this sample, viscosity increased rapidly and reached the same plateau value, independent of crystallization temperatures in the 35−45 °C range. From all indications as shown in Figure 9A, the nearly identical plateau value suggests a solid sample has been achieved. It was found that the viscosity development of other PHMA-rich samples with 15−50 wt% PHMA are identical with that shown in Figure 9A. The ultimate viscosity value for the PHMA-rich phase is exactly the same, independent of blend composition and crystallization temperature, as shown in Figure 10.

Viscosity development as a function of temperature and time for the PHMA-poor phase is quite different from the observations reported above. Here the viscosity increase is extremely sensitive to crystallization temperature in the range 35−45 °C. At lower crystallization temperatures, the viscosity increases abruptly and quickly reaches plateau values. With increasing crystallization temperatures in the range from 35 to 45 °C, viscosity development becomes slower and reaches a lower

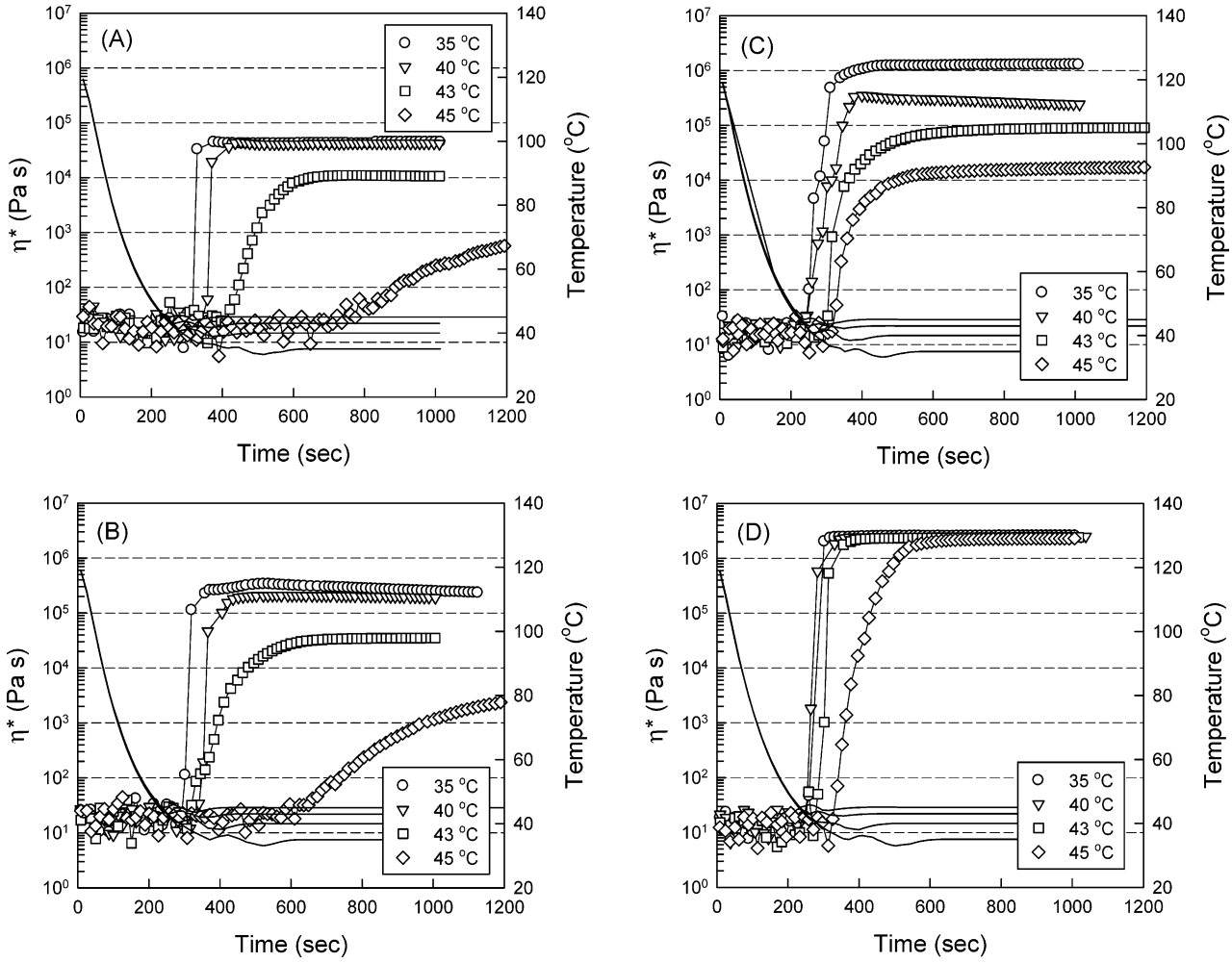

Figure 7. Viscosity development of PHMA/PPG blends crystallized isothermally at various temperatures of 35−45 °C: (A) 10 wt% PHMA, (B) 20 wt% PHMA, (C) 40 wt% PHMA, and (D) 50 wt% PHMA. Solid lines indicate temperature profiles.

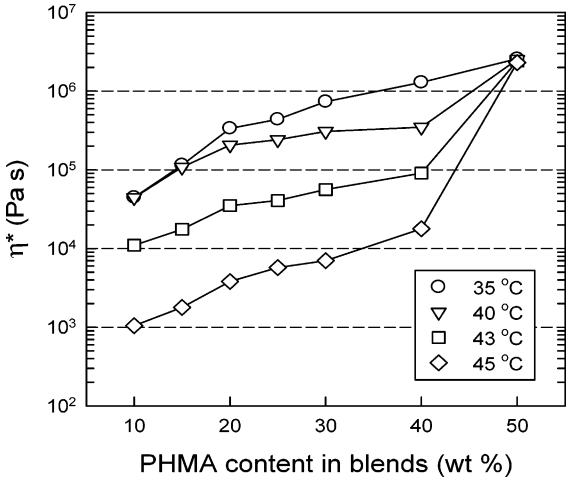

Figure 8. Ultimate complex viscosity (η^*) of PHMA/PPG blends as a function of blend compositions at various crystallization temperatures of 35−45 °C.

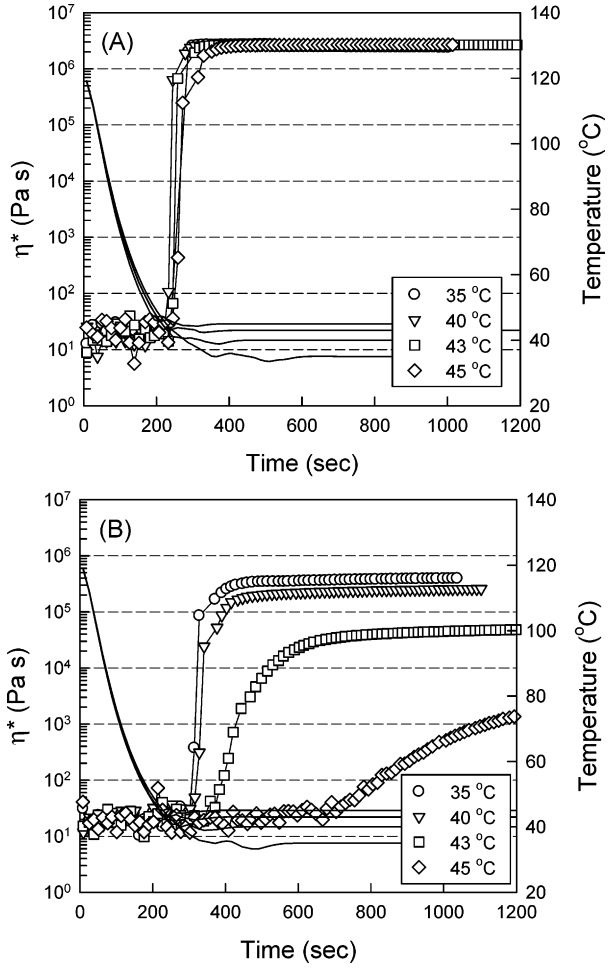

Figure 9. Typical viscosity development in the PHMA-rich phase (A) and the PHMA-poor phase (B), which are obtained from PHMA/PPG blend with 10 wt% PHMA crystallized isothermally at various temperatures of 35−45 °C. Solid lines indicate temperature profiles.

plateau value, as shown in Figure 9B. The time-dependent viscosity development was observed as almost identical for all the PHMA-poor phase in blends with 10−50 wt% PHMA content. The only difference is the ultimate viscosity. As shown in Figure 10, the ultimate viscosity value for each crystallization temperature increases with PHMA content and decreases in rate with increasing crystallization temperature. As expected, this

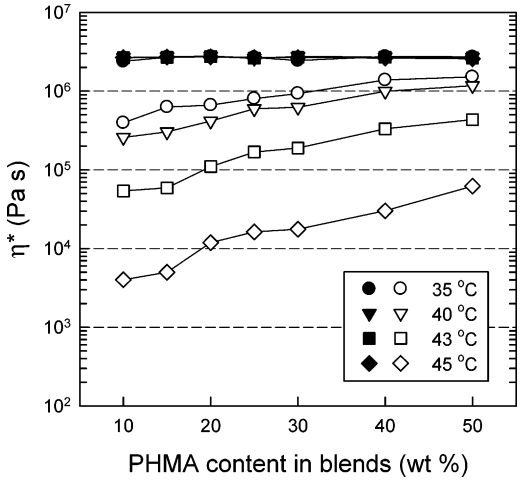

Figure 10. Ultimate complex viscosity (η^*) of the PHMA-rich phase (filled symbols) and the PHMA-poor phase (open symbols) as a function of PHMA/PPG blend composition at various crystallization temperatures of 35−45 °C.

is due to the fact that the PHMA content (Table 1) as well as degree of crystallinity (Figure 6) in the PHMA-poor phase increases with the overall PHMA content, resulting in the higher ultimate viscosity at higher PHMA blend content. The time evolution of the viscosity differs significantly for the two types of samples. A simple explanation is to attribute these differences to the PHMA content in both phases.

When the viscosity development of the blend with 10 wt% PHMA (Figure 7A) is compared with that of respective PHMA-rich and PHMA-poor phases (Figure 9), several interesting facts emerge. The viscosity increase for the 10 wt% blend is nearly identical to that obtained for the PHMA-poor phase. As described above, the PHMA-rich phase is fully solidified at all crystallization temperatures. In contrast, the PHMA-poor phase may remain in the molten state for a time period after reaching the crystallization temperature. When the small-amplitude oscillatory shear force is applied to the blend samples, the PHMA-poor phase responds accordingly. PHMA-poor phase-driven viscosity development is observed for all blends with lower PHMA content up to 40 wt%. As noted above, with increasing the PHMA content in the blend, the contribution of the PHMA-rich phase dominates viscosity development (Figure 7).

The ultimate viscosity of the blend with 10 wt% PHMA at all crystallization temperatures of 35−45 °C is lower than the values of the PHMA-poor phase. This result is unexpected as the degree of crystallinity (2.8−5.7%) of the blend at various crystallization temperatures of 35−45 °C is significantly higher than that (0.3−3.1%) of the PHMA-poor phase. It is therefore believed that the ultimate viscosity is dependent on not only the degree of crystallinity in the overall blend but also the interaction between domains (PHMA-rich phase) and the matrix (PHMA-poor phase). A magnified optical image of the blend with 10 wt% PHMA is shown in Figure 11. The morphological features of domains (PHMA-rich phase) and matrix (PHMA-poor phase) are quite different. For the blend with 10 wt% PHMA, the degree of crystallinity is 39.8−45.3% for the PHMA-rich phase domains and 0.3−3.1% for the PHMA-poor phase matrix at all crystallization temperatures of 35−45 °C. There is a liquid/liquid phase-separated structure even above melting temperature. A sharp interface exists between the dispersed domains and matrix. Even after the overall blend has crystallized, the interface between domains and matrix appears to remain disconnected, as can be seen in Figure 11. Therefore,

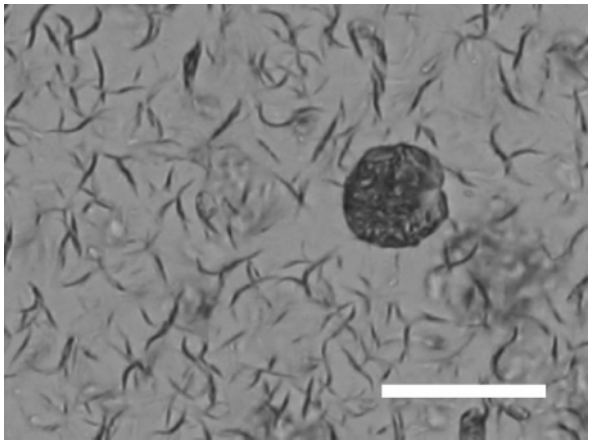

Figure 11. Optical micrograph of the PHMA/PPG blend with 10 wt% PHMA. The scale bar is 50 μm.

when the external small-amplitude oscillatory shear force is applied, there is interfacial slippage between the domains and matrix for the blends.[22,23] This is true for all blends with lower PHMA content.

It is interesting to note that the PHMA-poor phase matrix achieves an extremely high viscosity at such crystallinity after the sample has fully crystallized. A closer examination of the PHMA/PPG blends reveals that "curved-leaf"-shaped or "needle"-shaped crystallites have developed in the PHMA-poor phase, as seen in Figure 11. This type of crystalline structure certainly contributes very differently to sample viscosity. In addition, these crystallites seem to be interconnected as seen in Figure 11. It is our belief that the percolated morphology of "curved-leaf"-shaped crystallites yields the exceptional high ultimate viscosity (Figure 9B) even for samples with a very low degree of crystallinity in the PHMA-poor phase. In this crystallization process, PHMA chains diffuse to nuclei to form the "curved-leaf"-shaped crystallites. These diffusing PHMA chains to nuclei serve as connecting molecules between the crystallites and amorphous region, unlike the sharp interface between PHMA-rich phase domains (hard spheres) and PHMA-poor phases due to liquid/liquid-phase separation. It is believed that these interconnecting PHMA chains also provide the enhanced ultimate viscosity.

Conclusions

The viscoelastic physical gelation of immiscible and crystallizable blends, composed of crystallizable PHMA and non-crystallizable PPG, has been explained in terms of the crystallization process, microstructural features, and interaction between domains and matrix. All PHMA/PPG binary blends prepared in this study exhibited a phase-separated structure with PHMA-rich and PHMA-poor phases. Blend morphology varies from the dispersed domains−continuous matrix to a bicontinuous morphology with increasing the PHMA content in the blend. The local composition, morphological features, quiescent crystallization, and physical gelation process were characterized using ^{1}H NMR, optical microscopy, differential scanning calorimetry, and small-amplitude oscillatory viscometry, respectively. The local composition and crystallinity in PHMA-rich and PHMA-poor phases were varied, depending on blend composition and/or crystallization temperature. The viscoelastic gelation process for blends with low PHMA content of 10−40 wt% was dominated by crystallization in the PHMA-poor phase. The ultimate viscosity of the overall blend was also lower than that of the PHMA-poor phase. The high ultimate viscosity in the PHMA-poor phase was associated with the percolated morphology of "curved-leaf"-shaped crystallites. For blends with above 40 wt% PHMA, the contribution of the PHMA-rich phase increases for the physical gelation process in the PHMA/PPG blends. Viscosity development of the blend with 50 wt% PHMA is dominated by the bicontinuous morphology.

Acknowledgment. The authors thank the Environmental Protection Agency (TSE Grant #RD831636010) and the New England Green Chemistry Consortium (NEGCC) for financial support. We are also appreciative of a grant from National Starch & Chemical, a subsidiary of ICI, in support of this research.

References and Notes

(1) Olabisi, O.; Robeson, L. M.; Shaw, M. T. *Polymer−Polymer Miscibility*; Academic Press: New York, 1979.
(2) Utracki, L. A., Ed. *Polymer Blends Handbook*; Kluwer Academic Publishers: Boston, 2002.
(3) Paul, D. R., Bucknall, C. B., Eds. *Polymer Blends*; John Wiley & Sons: New York, 2000.
(4) Szycher, M. *Szycher's Handbook of Polyurethanes*; CRC Press: Boca Raton, FL, 1999.
(5) Jeong, Y. G.; Hashida, T.; Hsu, S. L.; Paul, C. W. *Macromolecules* **2005**, *38*, 2889−2896.
(6) Jeong, Y. G.; Ramalingam, S.; Archer, J.; Hsu, S. L.; Paul, C. W. *J. Phys. Chem. B* **2006**, *110*, 2541−2548.
(7) Duffy, D. J.; Stidham, H. D.; Hsu, S. L.; Sasaki, S.; Takahara, A.; Kajiyama, T. *J. Mater. Sci.* **2002**, *37*, 4851−4859.
(8) Jeong, Y. G.; Hashida, T.; Wu, G.; Hsu, S. L.; Paul, C. W. *Macromolecules* **2006**, *39*, 274−280.
(9) Duffy, D. J.; Heintz, A. M.; Stidham, H. D.; Hsu, S. L.; Suen, W.; Chu, W.; Paul, C. W. *J. Adhes.* **2003**, *79*, 1091−1107.
(10) Hashida, T.; Jeong, Y. G.; Hua, Y.; Hsu, S. L.; Paul, C. W. *Macromolecules* **2005**, *38*, 2876−2882.
(11) Jeong, Y. G.; Hashida, T.; Wu, G.; Hsu, S. L.; Paul, C. W. *Macromolecules* **2006**, *39*, 274−280.
(12) Richtering, H. W.; Gagnon, K. D.; Lenz, R. W.; Fuller, R. C.; Winter, H. H. *Macromolecules* **1992**, *25*, 2429−2433.
(13) Acierno, S.; Grizzuti, N.; Winter, H. H. *Macromolecules* **2002**, *35*, 5043−5048.
(14) Pogodina, N. V.; Winter, H. H. *Macromolecules* **1998**, *31*, 8164−8172.
(15) Gelfer, M.; Horst, R. H.; Winter, H. H.; Heintz, A. M.; Hsu, S. L. *Polymer* **2003**, *44*, 2363−2371.
(16) Kelarakis, A.; Mai, S.-M.; Booth, C.; Ryan, A. J. *Polymer* **2005**, *46*, 2739−2747.
(17) Horst, R. H.; Winter, H. H. *Macromolecules* **2000**, *33*, 130−136.
(18) Palierne, J. F. *Rheol. Acta* **1990**, *29*, 204−214.
(19) Lacroix, C.; Bousmina, M.; Carreau, P. J.; Favis, B. D.; Michel, A. *Polymer* **1996**, *37*, 2939−2947.
(20) Scholz, P.; Froelich, D.; Muller, R. *J. Rheol.* **1989**, *33*, 481−499.
(21) Boutahar, K.; Carrot, C.; Guillet, J. *Macromolecules* **1998**, *31*, 1921−1929.
(22) Narayanan, B.; Pryamitsyn, V. A.; Ganesan, V. *Macromolecules* **2004**, *37*, 10180−10194.
(23) Zhao, R.; Macosko, C. W. *J. Rheol.* **2002**, *46*, 145−167.
(24) Kitade, S.; Ichikawa, A.; Imura, N.; Takahashi, Y.; Noda, I. *J. Rheol.* **1997**, *41*, 1039−1060.
(25) Aylwin, P. A.; Boyd, R. H. *Polymer* **1984**, *25*, 323−329.
(26) Qian, C.; Mumby, S. J.; Eichinger, B. E. *Macromolecules* **1991**, *24*, 1655−1661.
(27) Krishnamoorti, R.; Graessley, W. W.; Balsara, N. P.; Lohse, D. J. *J. Chem. Phys.* **1994**, *100*, 3894−3904.
(28) Lodge, T. P.; Mcleish, T. C. B. *Macromolecules* **2000**, *33*, 5278−5284.
(29) Jinnai, H.; Hashimoto, T.; Lee, D.; Chen, S.-H. *Macromolecules* **1997**, *30*, 130−136.

MA060666Z